Journal of MATERIALS RESEARCH

Article
DOI:10.1557/s43578-022-00805-w

# Silk fibroin fibers-based shape memory membrane with Janus wettability for multitiered wearable protection

Yue Zhang[1,b)], Jiahui Zhou[1,b)], Heli Deng[1], Ying Fang[1], Na Qiao[1], Meng Ren[1], Yufan Zhang[4], Desuo Zhang[1,2], Hong Lin[1], Yuyue Chen[1,a)], Ken Tye Yong[3,a)], Jiaqing Xiong[4,a)]

[1] College of Textile and Clothing Engineering, Soochow University, Suzhou 215123, China
[2] National Engineering Laboratory for Modern Silk, Soochow University, Suzhou 215123, China
[3] School of Biomedical Engineering, The University of Sydney, Sydney, NSW 2006, Australia
[4] Innovation Center for Textile Science and Technology, Donghua University, Shanghai 201620, China
[a)] Address all correspondence to these authors. e-mails: chenyy@suda.edu.cn; ken.yong@sydney.edu.au; jqxiong@dhu.edu.cn
[b)] These authors have contributed equally to this work.

Received: 17 June 2022; accepted: 24 October 2022; published online: 31 January 2023

**Realizing breathable shape memory fiber-based material with antibacterial and waterproof performances is important for multitiered wearable protection to address the increasing concerns of air pollution. Herein, using an alternating electrospinning-electrospraying technology, we develop a fiber-based membrane with Janus wettability based on a silk fibroin nanofibers-substrate (SFNFs), a polyurethane nanospheres-top layer (PUNSs), and a middle layer of PU nanofibers-mat with in-situ grown silver nanoparticles (PUNFs-AgNPs), which serves separately for skin contact, a self-cleaning physical barrier to resist external aerosol/bacteria (PM2.5 filtration efficiency ~ 98.1%), and a bio-barrier that can sterilize harmful particles and inhibit bacteria proliferation (> 95%). This breathable Janus film (SFNFs/PUNFs-AgNPs/PUNSs, SPAP) with an antibacterial filter shows shape memory stretchability enabled by the thermoplastic PU component, which is mechanically adaptive to human body for wearable protection. This work presents a breathable wearable material for air-filtration and anti-bacteria, promising for applications such as wound dressings, medical masks, protection suits, and multifunctional filters.**

## Introduction

The increasing air pollution in modern society has become a huge threat for our daily life, the global outbreak of coronavirus disease 2019 (COVID-19) is increasing this concern. The polluted air brings various contaminants such as smoke dust, PM2.5, bacteria, and viruses, which are commonly accompanied by fog, moisture, and exhalation and behave as aerosol spread everywhere to cause severe health threats on human beings [1, 2]. More seriously, the polluted aerosol would cause various health problems such as skin allergy, respiratory diseases, as well as pandemics, endangering people's lives and disrupting the normal functioning of society [3, 4]. As the aerosol surrounds us all the time, a functional textile that is mostly in contact with the human body would be one of the most promising materials for wearable protection.

Important progress of functional textile has been achieved in the governance of air pollution, including daily textiles and non-woven fabrics [5–8] that are either anti-bacterial [9], anti-viral [2], or can filtrate the dust such as PM2.5 [10], which usually behave as single function, either show insufficient skin affinity as well as poor mechanical compliance to accommodate the human body [11]. Moreover, most of the threats in the air move accompanied by the moisture (small liquid droplets), which usually tend to be adsorbed and infiltrate the hydrophilic fabrics, increasing the filtration difficulty [12]. The important progress of this field inspires us that development of multifunctional materials to address all the challenges for wearable protection is important. The material with Janus wettability would be a good candidate to meet the application scenes required for wearable protection, which pursues favorable skin affinity,

waterproofness, and filtration capability. Stacking of different materials in virtue of electrospinning and electrospraying technologies promises a versatile strategy capable of constructing both architectures of nanofiber and microsphere [13], as well as integrating various components to realize the multifunctional material.

To this end, polymer components of silk fibroin (SF) and polyurethane (PU) with excellent processability were combined with in-situ silver nanoparticles (AgNPs) to construct a multifunctional membrane for human protection. SF is a fibrous protein with abundant non-polar amino acids [14], which shows unique mechanical and biological properties, such as high strength, flexibility biocompatibility, biodegradability and hydrophilicity, presenting favorable potential for skin contact application as well as for promoting wound healing [15]. However, SF is incompetent for the outer protection application due to its water solubility [16]. PU is a typical thermoplastic polymer that can impart the nano-/micro-fibers or spheres with elasticity to realize thermo-responsive shape memory property [17]. Meanwhile, PU shows intrinsic water resistance and good mechanical strength to serve as a protective layer to resist external threats. Accordingly, PU is a promising candidate to combine with SF to construct a membrane with Janus wettability [18]. In addition, as a traditional antibacterial agent, silver has the advantages of broad-spectrum and long-lasting antibacterial [19]. Especially silver nanomaterials have characteristics of the unique quantum effect, small size effect and large specific surface area [20], exhibiting super antibacterial capability and acceptable safety for human body [21]. Ag NPs have been increasingly applied for medical and healthcare, such as surgical instruments, wound antibacterial dressings [22] and artificial limbs [23].

Utilizing SF, PU, and AgNPs, this work presents an alternating electrospinning-electrospraying technique to develop a shape memory membrane with Janus wettability for multifunctional protection. The membrane appears as a sandwich structure with a hydrophilic bottom layer for skin contact and a hydrophobic top layer for screening the external moisture, between was inserted with an antibacterial filter for secondary filtration and antibacterial. Specifically, SF nanofibers (SFNFs) bottom layer was firstly fabricated by electrospinning, then PU with silver ion precursor was electrospun to deposit a layer of PU nanofibers (PUNFs) with AgNPs generated in-situ, followed by electrospraying a layer of PU nanospheres (PUNSs) to assemble into a sandwiched SFNFs/PUNFs-AgNPs/PUNSs (SPAP) membrane with Janus wettability. The hydrophilic SFNFs layer provides favorable air-permeability and skin affinity to act as a friendly biointerface. The PUNSs layer with intrinsic waterproofness and high surface roughness, serves as a superhydrophobic self-cleaning physical barrier to screen the invasive aerosol threats. The PUNFs/AgNPs filter with a high specific surface area ensures an additional bio-barrier for blocking and annihilating the bacteria. The Janus SPAP membrane shows shape memory stretchability and breathability for comfortable and attachable protection on human skin, exhibiting potential as versatile wearable protection materials for long-term usages.

## Results and discussion

### Fabrication and structure features of the SPAP membrane

Figure 1(a) presents the alternating process of electrospinning and electrospraying for fabrication of the SPAP membrane, allowing formation of nano/micro architectures of fibers or spheres. The morphology highly relies on the concentration and viscosity of the polymer solution [17, 24]. Figure 1(b) schematically shows the structure of SFNFs (bottom layer), PUNFs-AgNPs (middle layer), and PUNSs (top layer), respectively. SF is a kind of insoluble natural protein extracted from silkworm cocoon, which contains abundant amino acids necessary for human body, possessing a certain bacteriostasis and excellent biocompatibility, and has been widely applied for cosmetics, artificial skin, healthcare [25]. SFNFs layer enabled by electrospinning shows a mesh structure of nanofibers with high specific surface area, and it could exhibit high adsorption capacity and hydrophilicity (indicated by the inserted water contact angle (WCA) of $47.9° \pm 2.1°$) that are important for friendly contact with human skin. PU is a typical elastomer with good shape memory ability, competent for improving mechanical compliance of the SF layer for well accommodation with human body. The middle and top layer in [Fig. 1(b)] refers to a PUNFs-AgNPs layer and a PUNSs layer, which serve as a bio-barrier filter and a physical barrier, respectively. PUNSs layer with nanoparticles surface structure could deliver high surface roughness and superhydrophobicity (indicated by the inserted WCA of $152.9° \pm 1.3°$) to achieve self-cleaning performance. It is promising to be an outer barrier to resist the water, moisture, and vapour, blocking most of the pollutants from the air. Moreover, the PUNFs-AgNPs middle layer consisted of PU nanofibers with in-situ AgNPs reduced by N, N-dimethylformamide (DMF) solvent (see more details in Fig. S1, Supporting Information), could act as a bio-filter for both secondary aerosol filtration and bacteria inhabitation. Accordingly, the whole PSAP membrane shows a sandwiched structure with Janus wettability [Fig. 1(c)]. Owing to the shape memory PU component, the SPAP membrane could be configurated into various temporary shapes to adapt different substrates [Fig. 1(d)] and wearable applications.

### Morphology and geometrics of the SPAP membrane

Figure 2(a) shows macroscopic images of each layer of the SPAP membrane, wherein the three layers presented opaque

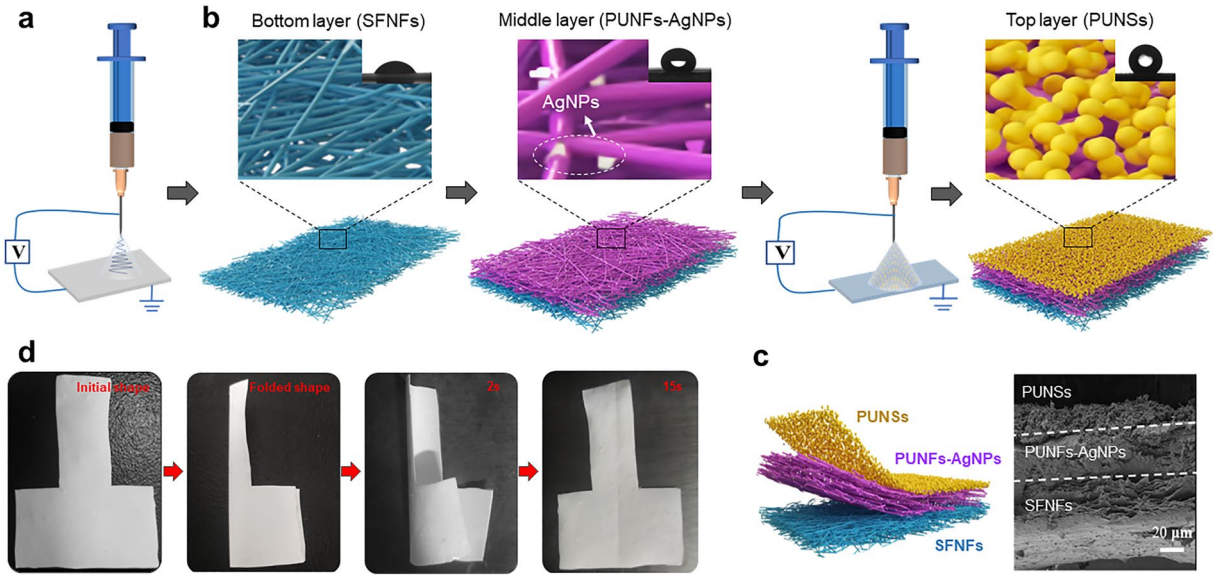


**Figure 1:** A Janus SPAP membrane with shape memory ability. (a, b) Schematic diagram of fabrication process of the SPAP membrane by electrospinning and electrospraying technologies. (c) Cross-section morphology of the SPAP membrane for demonstration of the sandwich structure. (d) Demonstration of the thermal shape memory ability of the SPAP membrane.

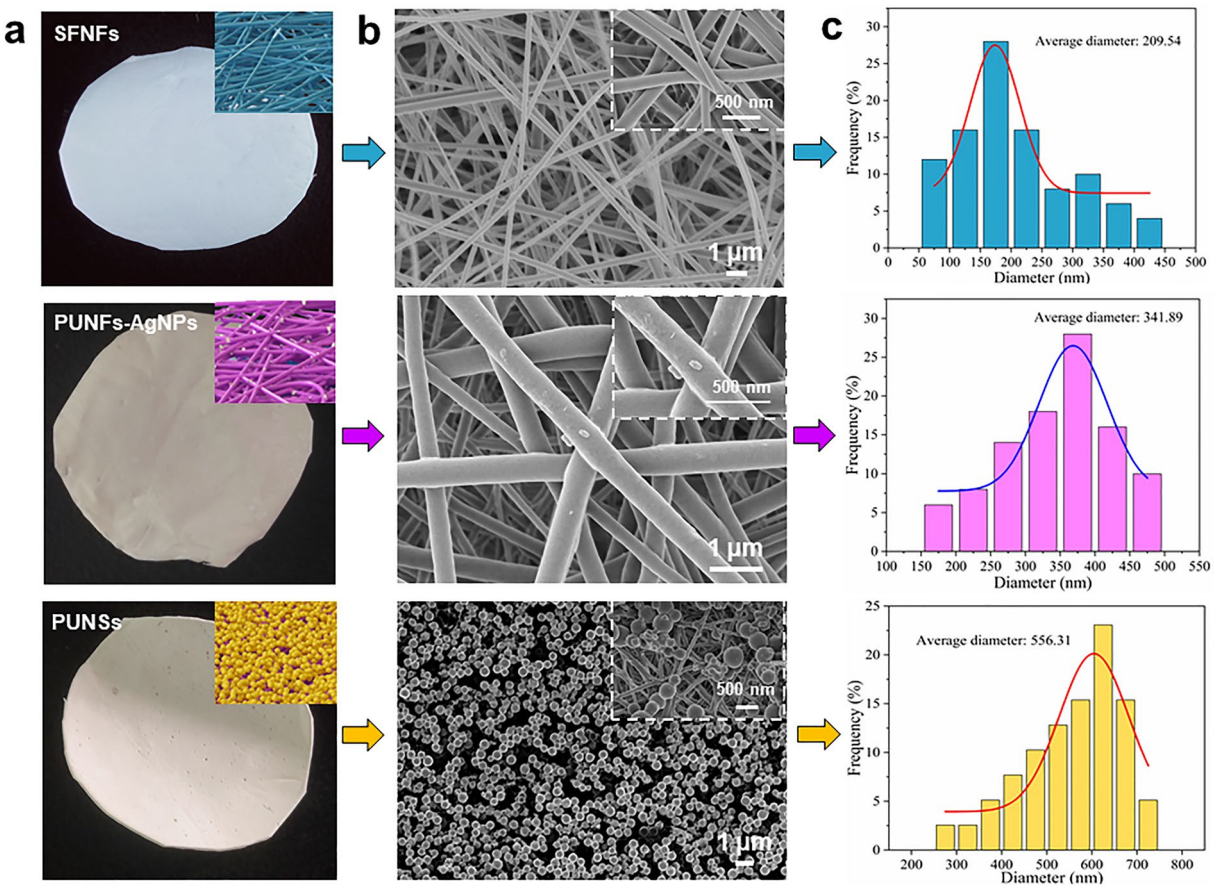


**Figure 2 :** Morphology and diameter distribution of each layer of the SPAP membrane. (a) Representative macroscopic images of the bottom (SFNFs), middle (PUNFs-AgNPs) and top (PUNSs) layer of the SPAP membrane. (b) SEM images showing the morphology of the bottom (SFNFs), middle (PUNFs-AgNPs) and top (PUNSs) layer of the SPAP membrane. (c) Diameter distribution of the SFNFs layer, PUNFs-AgNPs layer, and PUNSs layer.

appearance and uniform structure. Additionally, SFNFs layer showed a white color due to the high scattering of nanofibers, while the PUNFs-AgNPs layer presented a light brown color, indicating the AgNPs were generated in-situ. Moreover, the top view of the whole SPAP film also appeared as a light brown color, suggesting that a very thin PUNSs layer is sufficient to meet the roughness and superhydrophobicity requirements. The microscopic morphology and dimension of each layer were presented in [Fig. 2(b, c)]. Both SFNFs and PUNFs-AgNPs layers presented a highly porous 3D nanofiber network composed of randomly oriented fibers. AgNPs could be found on the surface of PUNFs [Fig. 2(b)], the exist Ag element was further proved on the cross section of the SPAP membrane by EDX test (Fig. S2, Supporting Information). It confirms the feasibility of this facile incorporation strategy of AgNPs free of post-reduction, avoiding damage of the nanofibers mesh. PUNSs showed an even morphology of nanospheres (diameter of ~ 700 nm), which are tightly attached to the fibers of the PUNFs-AgNPs layer [Fig. 2(b, c)]. The good mechanical adhesion could be attributed to the electrospraying process of PUNSs with high boiling point solvent (DMF), partially cured PUNSs would be generated and attached on the PUNFs-AgNPs substrate to realize a good interface stability, as well as improved surface roughness to attain good hydrophobicity.

## Properties of the SPAP membrane

The Fourier Transform Infrared Spectra (FTIR) of each layer of the SPAP membrane (SFNFs, PUNFs-AgNPs and PUNSs) is presented in [Fig. 3(a)]. The characteristic absorption bands at 1650–1660 $cm^{-1}$ (amide I), 1535–1545 $cm^{-1}$ (amide II), 1235 $cm^{-1}$ (amide III) are attributed to the SF with random coil or α-helix conformation (silk I), and the characteristic absorption bands at 1625–1640 $cm^{-1}$, 1515–1525 $cm^{-1}$, 1265 $cm^{-1}$ are attributed to the SF with β-sheet structure conformation (silk II) [26, 27]. Because of the treatment with 75% (v/v) ethanol vapor, the SFNFs layer spectrum displayed the characteristic peaks at 1625 $cm^{-1}$, 1514 $cm^{-1}$, 1232 $cm^{-1}$, indicating a strong β-sheet structure conformation [28]. The characteristic absorption peak of the PUNSs layer at 3330 $cm^{-1}$ belongs to the N–H stretching vibration, the broad peak at 2957 $cm^{-1}$ corresponds to the stretching vibration of C–H groups, the sharp peak at 1727 $cm^{-1}$ represents the C=O stretching vibration of urethane groups, while the peak at 1528 $cm^{-1}$ and 1079 $cm^{-1}$ belong to the N–H bending vibration and the C–O–C stretching vibrations [29]. The PUNFs-AgNPs layer showed a similar spectrum, indicating AgNPs are physically covered on the PU nanofibers network.

Figure 3(b) shows the thermal property of SFNFs, PUNSs, PUNFs-AgNPs and the SPAP membrane, the weight loss ratio of the SPAP membrane complied well with the initial ratio of

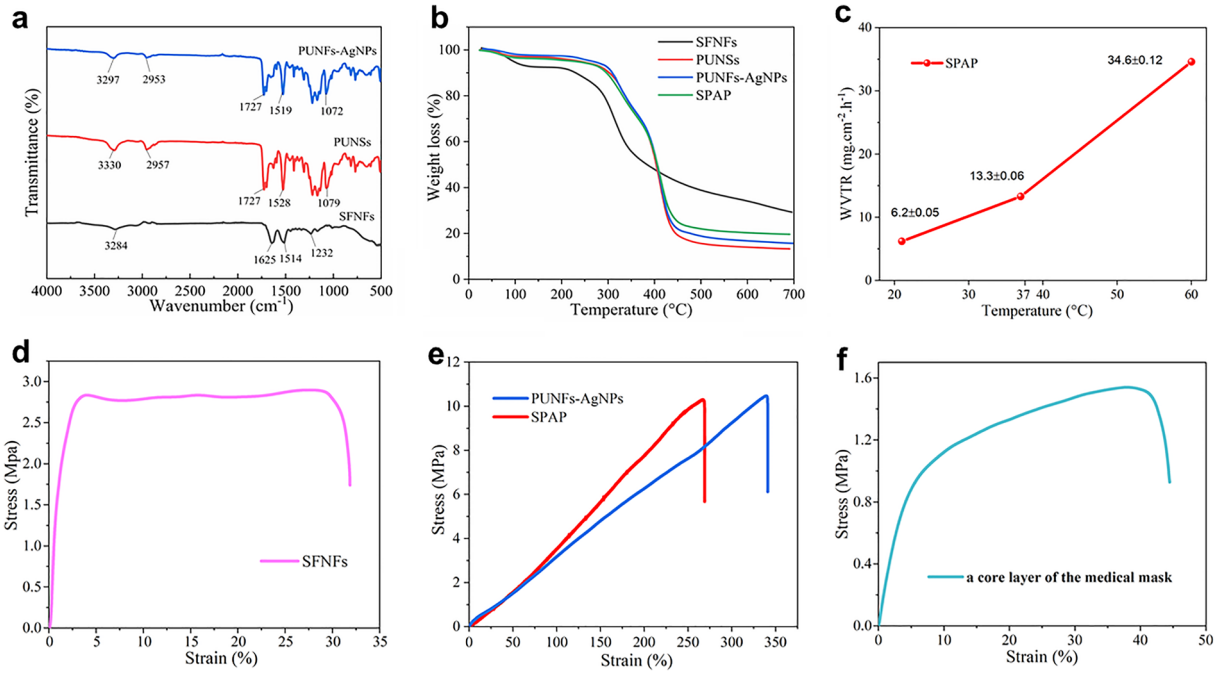


**Figure 3:** Properties of the SPAP membrane. (a) FTIR analysis of the SFNFs, PUNFs-AgNPs and PUNSs layer. (b) TGA thermal stability of SFNFs, PUNFs-AgNPs, PUNSs and the SPAP membrane. (c) Water vapor transmission rate (WVTR) of the SPAP membrane under different temperatures with constant humidity (60 ± 3%). (d–f) Comparison of the stress–strain properties of (d) SFNFs, (e) PUNFs-AgNPs, SPAP, and (f) the control sample of a core layer of the commercial medical mask (a melt-blown fabric).

each component, the char yields after the pyrolysis of SFNFs, PUNSs, PUNFs-AgNPs and the SPAP membrane as a result of the residual nonvolatile carbonaceous material in the heating process are about 29.3%, 13.3%, 15.7% and 19.6% [30]. The thermal decomposition temperature was all above 200℃, indicating that all the components are adoptable for most of the application scenarios. SFNFs layer showed a little bit lower thermal stability, but the PU component could effectively improve the thermal stability of the SPAP membrane. Therefore, the coupling of SFNFs and PU is an effective way to achieve a thermostable wearable material.

WVTR is important to wearable protective materials, and especially are required for mask and would healing. Because the low WVTR can induce bacterial growth and cause an uncomfortable feeling of wearing, while the high WVTR can maintain drying of the wound and skin as well as improve the protection effect. Evaporation of water through the SPAP membrane was examined by monitoring the weight loss of the cup for 3 days. The final WVTR was calculated according to the equation (1).

$$WVTR\ of\ the\ SPAP = \frac{water\ weight\ change(mg)}{the\ SPAP\ exposure\ area\ (cm^2) \times exposure\ time(h)}, \quad (1)$$

where numerator is the change in the amount of the water weight (mg), and denominator is the product of exposure area ($cm^2$) of the sample and exposure time (h).

As shown in [Fig. 3(c)], the WVTR of SPAP membrane increased gradually as the temperature increased. The WVTR approximately ranged from 6.2 to 34.6 mg $cm^{-2}$ $h^{-1}$, which fully covered the suggested WVTR number ranging from 8.3 to 10.4 mg $cm^{-2}$ $h^{-1}$ around the body temperature [31]. The WVTR at 37 °C of the SPAP membrane was 13.3 ± 0.06 mg $cm^{-2}$ $h^{-1}$, better than the commonly used cambrayon (12.5 mg $cm^{-2}$ $h^{-1}$) [32]. It suggests that the SPAP membrane could well satisfy the application requirements of wearable protective materials.

Besides, the usage of wearable materials strongly relies on their mechanical properties because of the motorial behavior of skin [33]. The mechanical properties were evaluated by tensile tests at room temperature, a core layer of the commonly used medical mask was employed as a control sample for comparison [Fig. 3(d–f)]. As shown in [Fig. 3(d)], the SFNFs layer reached a maximum tensile stress of 2.8 MPa at 4% strain, which can sustain the tensile stress until to a breaking elongation of 31%. In comparison, the PUNFs-AgNPs film showed a much higher tensile performance that achieves 10 MPa at 350% tensile strain [Fig. 3(e)]. Because of the superior mechanical properties of the PU component, the SPAP membrane can sustain tensile stress of 10 MPa and breaking elongation of 270%. It suggests that the PU component could effectively restrain the SFNFs during stretching, allowing displacement between the fibers free of damage. It demonstrates that the combination of SF and PU is an effective way to achieve a Janus membrane with good mechanical performances. As a control sample shown in [Fig. 3(f)], a melt-blown fabric of the middle layer of medical masks can only sustain tensile stress of ~ 1.6 MPa as well as 40% breaking elongation, further confirming the mechanical superiorities and application potential of the SPAP membrane.

## Self-cleaning and shape memory properties

Usually, higher surface roughness and WCAs could be achieved on micro-nano hierarchical surfaces. Materials with low surface energy and high surface roughness could provide higher WCAs [34, 35]. Materials with a WCA between 150° and 180° are regarded as superhydrophobic surfaces, which usually show water repellency, antifogging, antifouling, and self-cleaning properties [36]. As proved in [Fig. 4(a)], the bottom layer (SFNFs) is an insoluble material but presented a WCA of 47.9° ± 2.1°, indicating it is a hydrophilic interface which has good skin affinity and biological characteristics, favorable for skin contact. The middle layer of the SPAP membrane (PUNFs-AgNPs) showed a WCA of 136.7° ± 1.1°, and the hydrophobicity was attributed to the intrinsic waterproofness of PU as well as the rough surface constructed by nanofibers. However, this hydrophobicity was insufficient to ensure favorable functions in antifouling and self-cleaning. To improve the protection capability, another top layer of PU nanospheres (PUNSs) was deposited on the PUNFs-AgNPs nanofibers, creating a hierarchical structure with higher surface roughness. It showed an improved WCA of 152.9° ± 1.3° to realize superhydrophobicity that is competent in resisting the external threat such as water and moisture [37]. Self-cleaning properties of the SPAP membrane were evaluated using carbon powders as the simulated contaminants. Figure 4(b) presents the SPAP surface covered with carbon powders can be facilely cleaned by the water droplets within 3 s, rendering the granular contaminants in a dry state or accompanied by moisture could not long stay on the surface, thus promoting the protection [38].

Stretchability of materials is important in wearable applications to adapt mechanical deformation of human skin. For a multilayered membrane, its stretchability highly relies on the interface stability between different layers. Herein, the alternating electrospinning-electrospraying technology stacks the functional materials layer by layer, capable of providing good interface anchoring and intermolecular force that are important for improving the interface adhesion between different layers of the SPAP membrane. As shown in [Fig. 4(c)], the SPAP membrane showed great recovery upon tensile loading–unloading cyclic tests at a strain of ~ 30%, suggesting the good interface stability of SPAP and high capability for energy dissipation enabled by the stretchable PU component [39]. The reduced Young

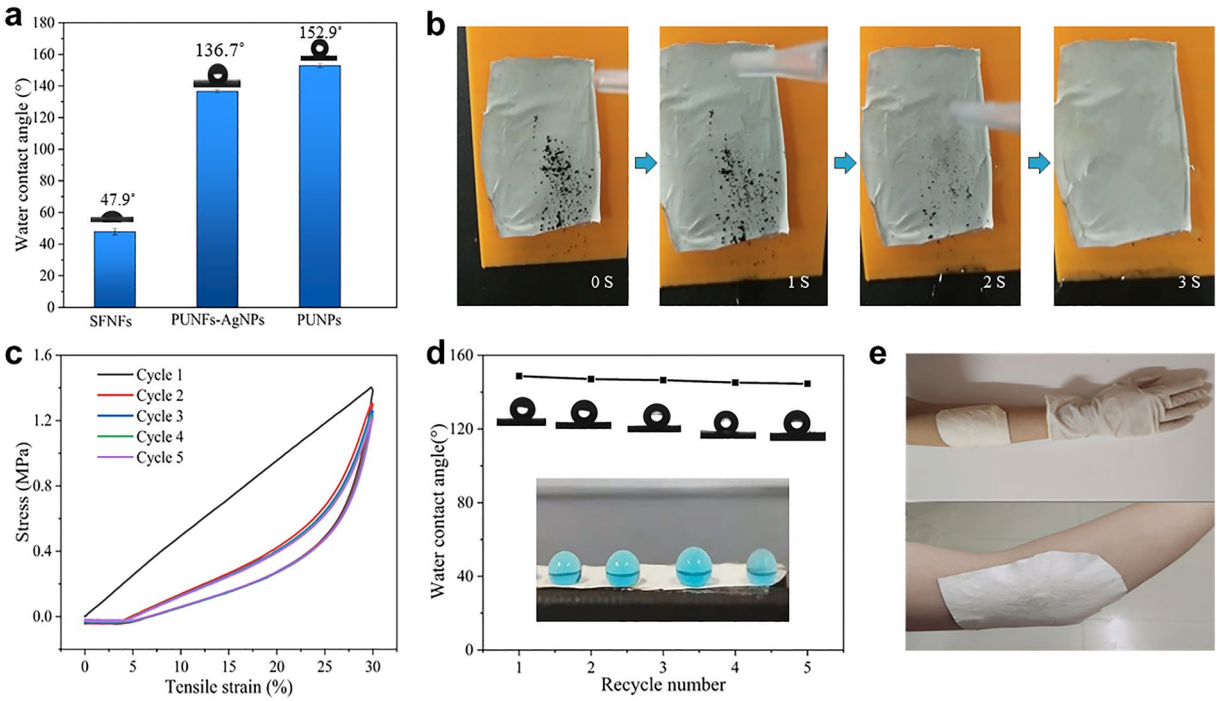


**Figure 4:** Self-cleaning, stretchability and mechanical stability of the SPAP membrane. (a) WCA of SFNFs, PUNFs-AgNPs and PUNSs layer. Error bars represent twice of the standard deviations (SD). (b) Photograph demonstration of self-cleaning performance. (c) Cyclic elasticity of the SPAP membrane. (d) Variations in WCA of the SPAP membrane after each cycle of stretching (30% strain), inset is a photograph of water droplets resting on the surface of the stretched SPAP membrane at 30% strain. (e) Photograph demonstration of the SPAP membrane conformally attached on forearm and elbow joint.

modulus after the first cycle is attributed to the destruction of weak net-points between fibers in the initial cycle, thereafter, it transformed into an elastic network with a relative stability. The slight residual strain for each cycle was observed, which is due to the inherent thermoplasticity of PU, in which energy was dissipated for the polymer chains disentanglement [40]. Even so, the SPAP membrane shows excellent recovery that imparts its good application potential for wearables. Meanwhile, stable superhydrophobicity of the SPAP membrane was verified after five cycles of a tensile test at the strain of 30% [Fig. 4(d)], inset was a photograph of water droplets resting on the surface of the SPAP membrane after five cycles of stretching, the stable hydrophobicity suggests durable wearable applications can be achieved. Figure 4(e) demonstrates the reconfigurability of the SPAP membrane by its shape memory ability, it can be conformably attached on forearm and elbow joints, adapting applications for different curvatures of human body.

## PM2.5 filtration performance

PM2.5 is one of the biggest threats for human beings, achieving PM2.5 filtration is of great importance for wearable protection materials. Typically, the pollutant particles produced by burning sandalwood were used as the model particulate matter (PM) pollutant [41]. Specifically, sandalwood combustion acted as a model system of a PM2.5 source which contained various sizes of PM particles and other components similar to those of exhaust gas, such as CO, $NO_2$, $SO_2$, and volatile organic compounds (VOCs), e.g., benzene, aldehydes, polycyclic aromatic hydrocarbons, etc. [42]. A PM2.5 filtration experiment was carried out as shown in [Fig. 5(a)], the model PM pollutant was placed on the inlet side of a PM counter sensor, which was connected to the computer to record the real-time PM2.5 density at the outlet [43]. The SPAP membrane and commercial medical mask were applied to block the inlet, the detected PM2.5 densities with and without filter were employed to calculate the filtration efficiency, the test was performed continuously for 45 s and calculated the filtration efficiency every five minutes. The smoke have a wide particle size distribution ranging from 300 nm to 10 mm, with the majority of particles being ~ 1 mm [44]. The filtration ability was confirmed by SEM as shown in [Fig. 5(b, c)], which revealed that the PSAP membrane can uniformly adsorb much more pollutant particles in comparison with the commercial medical mask. Accordingly, superior filtration efficiency (~ 98.1%) was delivered by the SPAP membrane rather than the commercial medical mask (~ 83.5%) [Fig. 5(d)], indicating the favorable potential for PM2.5 filtration [41, 45].

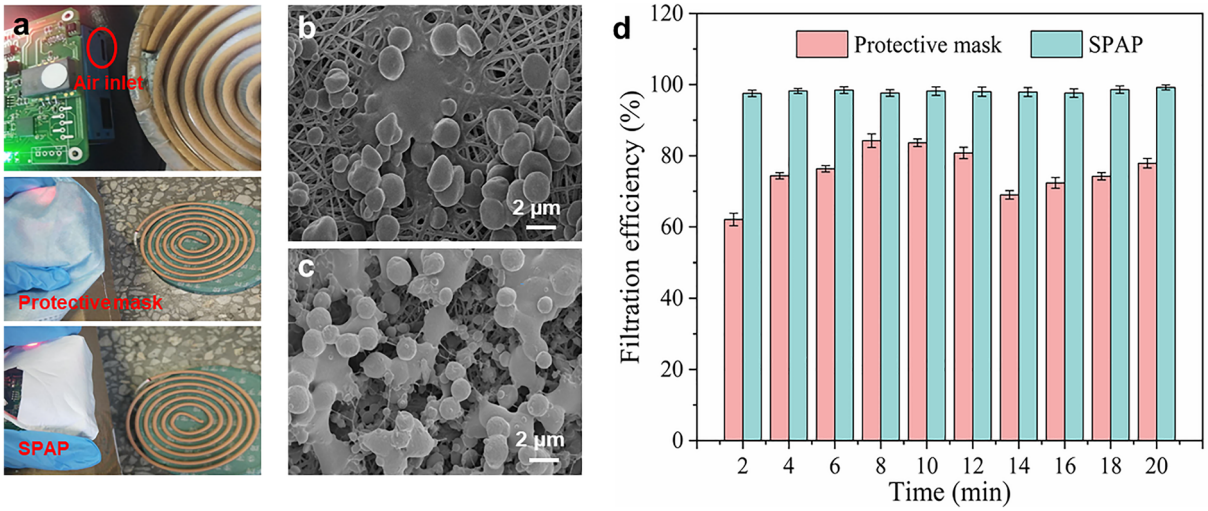


**Figure 5:** PM2.5 filtration ability of the SPAP membrane. (a) Photographs of the test set-up for PM2.5 filtration using commercial protective mask and the SPAP membrane as the filter. (b) SEM image of the commercial medical mask after PM2.5 filtration. (c) SEM image of the SPAP membrane after PM2.5 filtration. (d) Evolution of PM2.5 filtration efficiency of the SPAP membrane and the protective mask. Error bars represent twice of the standard deviations (SD).

## Antibacterial activity

As the superhydrophobicity and PM2.5 filtration ability only represent the physical shielding properties. The moisture or granular particles are commonly accompanied with the aerosol, which usually carry with abundant bacteria, bringing serious health threats to people [46]. Thus the bio-blocking ability of a wearable protection material is also quite significant. Herein, a qualitative test using antimicrobial ring was applied to evaluate antibacterial activity of the SPAP membrane. As shown in [Fig. 6(a)], compared with a commercial wound dressing without antibacterial properties, the inhibition zones can be observed around the SPAP membrane after incubation against negative (*E. coli*) and positive (*S. aureus*) bacteria. Figure 6(b) shows the diameter of inhibition zones measured using ImageJ, the SPAP membrane presented a satisfactory antibacterial activity, superior to the commercial wound dressing. To further

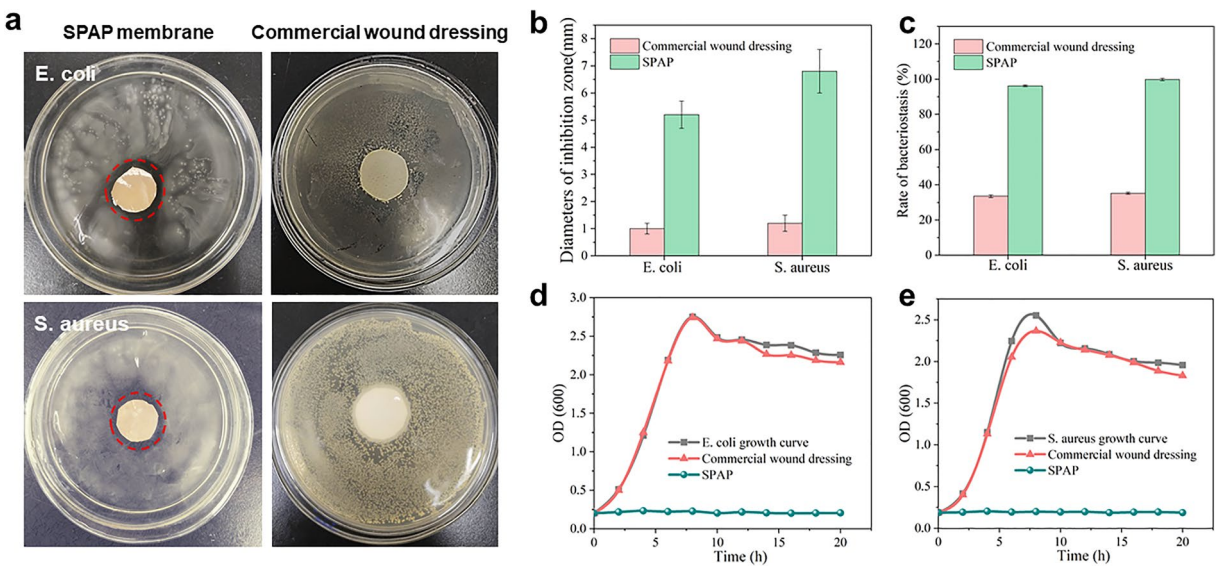


**Figure 6:** Antibacterial activity of the SPAP membrane. (a) Comparison of the antimicrobial rings of SPAP membrane and commercial wound dressing for *E. coli* and *S. aureus*. (b) Comparison of diameter of the antimicrobial ring of SPAP membrane and commercial wound dressing. (c) Comparison of bacteriostatic rate of SPAP membrane and commercial wound dressing. (d, e) Comparison of the growth curves of (d) *E. coli* and (e) *S. aureus* with commercial wound dressing and the SPAP membrane. Error bars represent twice of the standard deviations (SD).

improve the contact between the antibacterial material and the bacteriostatic liquid, a quantitative test of bacteriostatic rate was performed to accurately examine the antibacterial activity of the SPAP membrane [47]. The results of bacteriostatic rate are shown in the [Fig. 6(c)], indicating that the SPAP membrane has superior antibacterial effect (> 95%) compared with the commercial would dressings. Figure 6(d, e) present the OD values of bacteria within 20 h, much higher inhibitory effect for both *E. coli* and *S. aureus* can be observed on the SPAP membrane compared to that of the commercial would dressing. It indicates that the middle layer of PUNFs-AgNPs can function for antibacterial filters, ensuring the bio-filtration capability of the SPAP membrane for aerosol. The specific steps of the qualitative test of bacteriostatic ring and the quantitative test of bacteriostatic rate are referred to the supplementary notes.

## Conclusion

In a word, a multifunctional SPAP membrane was demonstrated by a facile alternating electrospinning and electrospraying technology. As a wearable protection material, the sandwiched SPAP membrane with Janus wettability delivers multiple protection abilities from outside to inside. The external two layers of PUNSs and PUNFs-AgNPs serves as physical barrier and bio-barrier, respectively, ensuring complete resistance to the water and moisture, as well as sufficient filtration for both PM2.5 and bacteria. It could well block most of the contaminants and hazardous substances which usually move along with the moisture and air. Moreover, the PUNFs-AgNPs filter enables additional antibacterial capability, avoiding the residual aerosol from the first screen further passing through the second layer, enhancing the protection effect. With the internal layer of SFNFs, the SPAP membrane is friendly for skin contact applications, promising for multifunctional wearable protection.

## Experimental section

### Materials

Cocoons of B. Mori silkworm were supplied by Jiaxing Silk Co., Ltd., China. Anhydrous sodium carbonate ($NaCO_3$) and lithium bromide (LiBr, 99%) were purchased from Jiangsu Qiangsheng Functional Chemical Co., Ltd., China. Dialysis tube ($M_W$ = 8000–14,000) was purchased from Suzhou Ketong Biomedical Technology Co., Ltd., China. Formic acid (98%) was purchased from Sinopharm Chemical Reagent Suzhou Co. Ltd., DMF (99.9%) was obtained from Shanghai Balinway Chemical Technology Co. Ltd., China. Thermoplastic PU ($M_W$ = 70,000) was purchased from Huntsman Chemical Trading (Shanghai) Co., Ltd., China. Silver nitrate ($AgNO_3$) was provided by Sinopac Chemical Reagent Suzhou Co. Ltd. All reagents are of analytical grade and were used without further treatment.

### Preparation of regenerated SF

The cocoons were degummed using the boiling sodium carbonate aqueous solution (0.5 wt%) for three times to remove the sericin proteins. After several times of rinses in deionized water the remaining sericin were removed, and dry at 40 ℃ to obtain the degummed silk fibroin. It was dissolved in lithium bromide solution (9.3 mol $L^{-1}$) at 60 ℃ for 2 h to reduce the degradation of silk fibroin during the dissolution process, and samples were dialyzed (molecular weight cut-off 14,000) against deionized water with change every 2 h. The dialyzed fibroin solution was lyophilized and stored at 4 ℃ until further use.

### Preparation of the spinning solution

First, the 12 wt% SF solution was prepared by dissolving the SF sponge in formic acid at room temperature with magnetic stirring for 12 h, the SF solution is used to produce the SFNFs (bottom layer of the SPAP). Then, 0.01 mol $L^{-1}$ silver nitrate DMF solution (1 wt%) was dropwise added into a 20 wt% PU solution (DMF solvent), followed by stirring at room temperature for 30 min, then heating the mixed solution at 80 °C for 10 min to reduce the silver ions into silver nanoparticles, so as to prepare the DMF solution of PU-AgNPs, and to produce the interlayer of the SPAP. Finally, 5 wt% PU solution was applied for electrospraying to fabricate the PUNSs layer.

### Production of the SPAP membrane

An alternating electrospinning and electrospraying process was applied to produce the SPAP. First, 12 wt% SF solution with feeding rate of 0.4 mL $h^{-1}$ was employed for electrospinning to fabricate the SF nanofibers, which was performed under an electrostatic filed of 25 kV and a working distance of 15 cm. With the same working parameters, 10 mL PU-AgNPs polymeric solution with a flow rate of 1 mL $h^{-1}$ was electrospun on the SFNFs membrane surface to produce a middle layer of PUNFs-AgNPs filter. At last, 5 wt% PU solution (0.8 mL $h^{-1}$) was deposited on the PUNFs-AgNPs layer by electrospraying, generating a layer of PUNSs. The produced SPAP membrane was treated with 75% (v/v) ethanol/water vapor to improve the β-sheet structure conformation (silk II) of SFNFs, followed by vacuum drying at 50 °C for 24 h to remove the residual solvent.

### Characterizations

The morphology of the SPAP membrane was investigated by scanning electron microscope (SEM, Hitachi S4800, Japan), and the diameter of the nanofibers or nanoparticles was measured by the software of ImageJ. The chemical composition of the SPAP membrane was tested using a Nicolet iS5 ATR

spectrophotometer (USA). The wettability of each layer of the SPAP membrane was inspected by the automatic video contact angle tester (KRUSS OCA30, Data Physics Instrument GmbH, Germany) using the sessile drop method under ambient condition, deionized water droplet of 3.0 μL was applied on the sample surface to record the static contact angle. Thermal decomposition was investigated by thermogravimetric analysis (SDT Q600, TA, USA) with a heating scan from room temperature to 700 °C, and the flow rate of nitrogen gas was fixed at 100 mL $min^{-1}$. Both mechanical properties and cyclic stretchability of SPAP membrane were evaluated using an INSTRON 5967 universal tensile tester based on the specimens with width of 5 mm, with speed of 5 mm $min^{-1}$ and clamps distance of 50 mm. The thickness of sample was measured by a micrometer (Nscing Es, China). For WVTR tests, the samples were covered on the permeability cup contained water at different temperatures to monitor the weight change of the setup, normalizing as WVTR, all the tests were performed by applying in triplicate at constant humidity of 60 ± 3%. A burning sandalwood was used to simulate the PM2.5 generator for filtration performance evaluation of the PSAP membrane. OriginPro95 (Origin lab, USA) software was applied for statistical analysis. Values were averaged and expressed as means ± standard deviation (SD). Statistical differences were determined by one-way ANOVA method and significance for all statistical analyses was set to $p < 0.05$.

### Antibacterial assessment

Referring to the standard GB/T 20944, the antibacterial ring was qualitatively tested by the AGAR plate diffusion method, and the antibacterial rate was quantitatively tested by the oscillatory method. The antibacterial properties of the SPAP membrane against common negative bacteria (*E. coli*) and positive bacteria (*S. aureus*) were studied.

## Acknowledgments

This work was supported by the Project funded by China Postdoctoral Science Foundation (No. 2019M661931), Prospective Application Research Project on Technology Innovation of Key Industries in Suzhou (No. SYG201936), MOE Key Laboratory of Advanced Textile Materials and Manufacturing Technology & Zhejiang Provincial Key Laboratory of Fiber Materials and Manufacturing Technology Research Project (No. 2019001). Post graduate Research &Practice Innovation Program of Jiangsu Province (KYCX20_2668).

## Data availability

Data will be made available on reasonable request.

## Declarations

**Conflict of interest** The authors declare that they have no conflict of interest.

## Supplementary Information

The online version contains supplementary material available at https://doi.org/10.1557/s43578-022-00805-w.

## References

1. A.P. Tai, M.V. Martin, CLJNCC Heald, threat to future global food security from climate change and ozone air pollution. Nat. Clim. Change **4**(9), 817–821 (2014)
2. Y. Si, Z. Zhang, W. Wu et al., Daylight-driven rechargeable antibacterial and antiviral nanofibrous membranes for bioprotective applications. Sci. Adv. **4**(3), eaar5931 (2018)
3. P. Perera Frederica, Multiple threats to child health from fossil fuel combustion: impacts of air pollution and climate change. Environ. Health Persp. **125**(2), 141–148 (2017)
4. X. Ma, T. Zhang, C. Ji, Y.Z. Hai, X. Shen, J. Hong, Threats to human health and ecosystem: Looking for air-pollution related damage since 1990. Renew. Sust. Energy Rev. **145**, 111146 (2021)
5. C. Liu, P.-C. Hsu, H.-W. Lee et al., Transparent air filter for high-efficiency PM 2.5 capture. Nat. Commun. **6**(1), 1–9 (2015)
6. R. Zhang, C. Liu, P.-C. Hsu et al., Nanofiber air filters with high-temperature stability for efficient PM2.5 removal from the pollution sources. Nano Lett. **16**(6), 3642–3649 (2016)
7. Y. Zhang, S. Yuan, X. Feng, H. Li, J. Zhou, B. Wang, Preparation of nanofibrous metal–organic framework filters for efficient air pollution control. J. Am. Chem. Soc. **138**(18), 5785–5788 (2016)
8. J. Xu, C. Liu, P.-C. Hsu et al., Roll-to-roll transfer of electrospun nanofiber film for high-efficiency transparent air filter. Nano Lett. **16**(2), 1270–1275 (2016)
9. Q.H. Qiu, S.Y. Chen, Y.P. Li et al., Functional nanofibers embedded into textiles for durable antibacterial properties. Chem. Eng. J. **384**(15), 123241 (2020)
10. B. Khalid, X. Bai, H. Wei, Y. Huang, H. Wu, Y. Cui, Direct blow-spinning of nanofibers on a window screen for highly efficient PM2.5 removal. Nano Lett. **17**(2), 1140–1148 (2017)
11. J.J. Xue, J.W. Xie, W.Y. Liu, Y.N. Xia, Electrospun nanofibers: new concepts, materials, and applications. Acc. Chem. Res. **50**(8), 1976–1987 (2017)
12. B. Niu, T. Hua, H.B. Hu et al., A highly durable textile-based sensor as a human-worn material interface for long-term multiple mechanical deformation sensing. J. Mater. Chem. C **7**(46), 14651–14663 (2019)
13. J.L. Sheng, Y. Li, X.F. Wang, Y. Si, J.Y. Yu, B. Ding, Thermal interfiber adhesion of the polyacrylonitrile/fluorinated polyurethane

nanofibrous membranes with enhanced waterproof-breathable performance. Sep. Purif. Technol. **158**, 53–61 (2016)
14. D.L. Heichel, J.A. Tumbic, M.E. Boch, A.W.K. Ma, K.A. Burke, Silk fibroin reactive inks for 3D printing crypt-like structures. Biomed. Mater. **15**(5), 055037 (2020)
15. D.W. Song, S.H. Kim, H.H. Kim, K.H. Lee, C.S. Ki, Y.H. Park, Multi-biofunction of antimicrobial peptide-immobilized silk fibroin nanofiber membrane: implications for wound healing. Acta Biomater. **39**(15), 146–155 (2016)
16. R.H. Wu, L.Y. Ma, C. Hou et al., Silk composite electronic textile sensor for high space precision 2D combo temperature-pressure sensing. Small **15**(31), 1901558 (2019)
17. J.Q. Xiong, H.S. Luo, D.C. Gao et al., Self-restoring, waterproof, tunable microstructural shape memory triboelectric nanogenerator for self-powered water temperature sensor. Nano Energy **61**, 584–593 (2019)
18. W.A. Yan, D.Y. Miao, A.A. Babar et al., Multi-scaled interconnected inter- and intra-fiber porous janus membranes for enhanced directional moisture transport. J. Colloid Interf. Sci. **565**, 426–435 (2020)
19. T. Akther, V. Mathipi, N.S. Kumar, M. Davoodbasha, H. Srinivasan, Environ. Sci. Pollut. R. **26**(13), 13649–13657 (2019)
20. S. Zhao, R.X. Jin, R.C. Jin, Opportunities and challenges in $CO_2$ reduction by gold- and silver-based electrocatalysts: from bulk metals to nanoparticles and atomically precise nanoclusters. ACS Energy Lett. **3**(2), 452–462 (2018)
21. G. Pagnotta, G. Graziani, N. Baldini et al., Nanodecoration of electrospun polymeric fibers with nanostructured silver coatings by ionized jet deposition for antibacterial tissues. Mater. Sci. Eng. C **113**, 110998 (2020)
22. M.A. Huq, Green synthesis of silver nanoparticles using *Pseudoduganella eburnea* MAHUQ-39 and their antimicrobial mechanisms investigation against drug resistant human pathogens. Int. J. Mol. Sci. **21**(4), 1510 (2020)
23. M. Behravan, A.H. Panahi, A. Naghizadeh, M. Ziaee, R. Mandavi, A. Mirzapour, Facile green synthesis of silver nanoparticles using *Berberis vulgaris* leaf and root aqueous extract and its antibacterial activity. Int. J. Biol. Macromol. **124**, 148–154 (2019)
24. Y. Li, J. Xiong, J. Lv et al., Mechanically interlocked stretchable nanofibers for multifunctional wearable triboelectric nanogenerator. Nano Energy **78**, 105358 (2020)
25. W.W. Huang, S.J. Ling, C.M. Li, F.G. Omenetto, D.L. Kaplan, Silkworm silk-based materials and devices generated using bionanotechnology. Chem. Soc. Rev. **47**(17), 6486–6504 (2018)
26. Z. Xue, Effect of microwave irradiation on the physical properties and structure of silk fibre. Fibres Text. East. Eur. **26**(130), 111–115 (2018)
27. D. Onofrei, T. Larson, K. Potfay, B. Blass, J. Ayon, G. Holland, Investigating the unique structure and physical properties of spider prey wrap silk with electron microscopy and solid-state NMR. Abstr. Pap. Am. Chem. Soc. **251**, 1155 (2016)
28. H. Tu, G.M. Wu, Y. Yi et al., Layer-by-layer immobilization of amphoteric carboxymethyl chitosan onto biocompatible silk fibroin nanofibrous mats. Carbohyd. Polym. **210**, 9–16 (2019)
29. S.M. Kim, H. Jeon, S.H. Shin et al., Superior toughness and fast self-healing at room temperature engineered by transparent elastomers. Adv. Mater. **30**(1), 1705145 (2018)
30. Y.H. Li, B. Zhou, G.Q. Zheng et al., Continuously prepared highly conductive and stretchable SWNT/MWNT synergistically composited electrospun thermoplastic polyurethane yarns for wearable sensing. J. Mater. Chem. C **6**(9), 2258–2269 (2018)
31. K.B. Escher, F.G. Shellock, An in vitro assessment of MRI issues at 3-tesla for antimicrobial silver-containing wound dressings. Ostomy Wound Manag. **58**(11), 22–27 (2012)
32. H.X. Wang, H. Zhou, X. Wei, H.T. Niu, T. Lin, Highly permeable, directional water transport cotton fabrics. Adv. Mater. Interfaces **5**(19), 1800815 (2018)
33. Z.J. Fan, B. Liu, J.Q. Wang et al., A novel wound dressing based on Ag/graphene polymer hydrogel: effectively kill bacteria and accelerate wound healing. Adv. Funct. Mater. **24**(25), 3933–3943 (2014)
34. H. Liu, Q.M. Li, Y.B. Bu et al., Stretchable conductive nonwoven fabrics with self-cleaning capability for tunable wearable strain sensor. Nano Energy **66**, 104143 (2019)
35. J. Xiong, M.F. Lin, J. Wang, S.L. Gaw, K. Parida, P.S. Lee, Wearable all-fabric-based triboelectric generator for water energy harvesting. Adv. Energy Mater. **7**(21), 1701243 (2017)
36. T. Zhu, Y. Cheng, J. Huang et al., A transparent superhydrophobic coating with mechanochemical robustness for anti-icing, photocatalysis and self-cleaning. Chem. Eng. J. **399**, 125746 (2020)
37. X. Chen, J. Xiong, K. Parida et al., Transparent and stretchable bimodal triboelectric nanogenerators with hierarchical micro-nanostructures for mechanical and water energy harvesting. Nano Energy **64**, 103904 (2019)
38. Y. Cheng, T.X. Zhu, S.H. Li et al., A novel strategy for fabricating robust superhydrophobic fabrics by environmentally-friendly enzyme etching. Chem. Eng. J. **355**, 290–298 (2019)
39. H.F. Lu, M. Wang, X.M. Chen, B.P. Lin, H. Yang, Interpenetrating liquid-crystal polyurethane/polyacrylate elastomer with ultrastrong mechanical property. J. Am. Chem. Soc. **141**(36), 14364–14369 (2019)
40. W.K. Liu, Y. Zhao, R. Wang et al., Post-crosslinked polyurethanes with excellent shape memory property. Macromol. Rapid Commun. **38**(23), 1700450 (2017)
41. X. Yang, Y. Pu, S.X. Li et al., Electrospun polymer composite membrane with superior thermal stability and excellent chemical resistance for high-efficiency PM2.5 capture. ACS Appl. Mater. Interfaces **11**(46), 43188–43199 (2019)
42. R.F. Zhang, C. Liu, P.C. Hsu et al., Nanofiber air filters with high-temperature stability for efficient PM2.5 removal from the pollution sources. Nano Lett. **16**(6), 3642–3649 (2016)

43. X.X. Huang, T.F. Jiao, Q.Q. Liu et al., Hierarchical electrospun nanofibers treated by solvent vapor annealing as air filtration mat for high-efficiency PM2.5 capture. Sci. China Mater. **62**(3), 423–436 (2019)
44. X.H. Yu, J. Pan, J. Zhang et al., A coaxial triboelectric nanogenerator fiber for energy harvesting and sensing under deformation. J. Mater. Chem. A **2017**(5), 6032–6037 (2017)
45. Q. Zhang, Q.J. Liang, Z. Zhang et al., Electromagnetic shielding hybrid nanogenerator for health monitoring and protection. Adv. Funct. Mater. **28**(1), 1703801 (2018)
46. J. Yan, M. Grantham, J. Pantelic et al., Infectious virus in exhaled breath of symptomatic seasonal influenza cases from a college community. Proc. Natl. Acad. Sci. USA **115**(5), 1081–1086 (2018)
47. B.L. Zhang, J.H. He, M.T. Shi, Y.Q. Liang, B.L. Guo, Injectable self-healing supramolecular hydrogels with conductivity and photo-thermal antibacterial activity to enhance complete skin regeneration. Chem. Eng. J. **400**, 125994 (2020)